sustainable chemistry

MDPI

Article

Evaluating the Ability of Bone Char/nTiO$_2$ Composite and UV Radiation for Simultaneous Oxidation and Adsorption of Arsenite

Susan Alkurdi [1,2], Raed Al-Juboori [3], Jochen Bundschuh [1,4,*] and Alla Marchuk [5]

1 School of Civil Engineering and Surveying, Faculty of Health, Engineering and Sciences, University of Southern Queensland, West Street, Toowoomba, QLD 4350, Australia; SusanAhmed78@gmail.com
2 Engineering Technical College, Northern Technical University, Kirkuk 36001, Iraq
3 Water Engineering Research Group, Department of Civil and Environmental Engineering, Aalto University, P.O. Box 15200, Aalto, FI-00076 Espoo, Finland; Raed.Al-Juboori@Aalto.fi
4 Doctoral Program in Science, Technology, Environment, and Mathematics, Department of Earth and Environmental Sciences, National Chung Cheng University, 168, University Rd., Min-Hsiung, Chia-Yi 62102, Taiwan
5 Centre for Sustainable Agricultural Systems, University of Southern Queensland, Toowoomba, QLD 4350, Australia; Alla.Marchuk@usq.edu.au
* Correspondence: Jochen.Bundschuh@usq.edu.au; Tel.: +61-7-4631-2694

Abstract: The reuse of waste materials for water treatment purposes is an important approach for promoting the circular economy and achieving effective environmental remediation. This study examined the use of bone char/titanium dioxide nanoparticles (BC/nTiO$_2$) composite and UV for As(III) and As(V) removal from water. The composite was produced via two ways: addition of nTiO$_2$ to bone char during and after pyrolysis. In comparison to the uncoated bone char pyrolyzed at 900 °C (BC900), nTiO$_2$ deposition onto bone char led to a decrease in the specific surface area and pore volume from 69 to 38 m^2/g and 0.23 to 0.16 cm^3/g, respectively. However, the pore size slightly increased from 14 to 17 nm upon the addition of nTiO$_2$. The composite prepared during pyrolysis (BC/nTiO$_2$)$_P$ had better As removal than that prepared after pyrolysis with the aid of ultrasound (BC/nTiO$_2$)$_{US}$ (57.3% vs. 24.8%). The composite (BC/nTiO$_2$)$_P$ had higher arsenate oxidation than (BC/nTiO$_2$)$_{US}$ by about 3.5 times. Arsenite oxidation and consequent adsorption with UV power of 4, 8 and 12 W was examined and benchmarked against the composite with visible light and BC alone. The highest UV power was found to be the most effective treatment with adsorption capacity of 281 µg/g followed by BC alone (196 µg/g). This suggests that the effect of surface area and pore volume loss due to nTiO$_2$ deposition can only be compensated by applying a high level of UV power.

Keywords: bone char; nTiO$_2$; pyrolysis; UV; visible light

Citation: Alkurdi, S.; Al-Juboori, R.; Bundschuh, J.; Marchuk, A. Evaluating the Ability of Bone Char/nTiO$_2$ Composite and UV Radiation for Simultaneous Oxidation and Adsorption of Arsenite. *Sustain. Chem.* **2022**, *3*, 19–34. https://doi.org/10.3390/suschem3010002

Academic Editor: Dimitrios Giannakoudakis

Received: 28 October 2021
Accepted: 22 December 2021
Published: 8 January 2022

1. Introduction

Elevated arsenic concentration in ground water is a global concern that affects not only drinking water availability, but also food safety [1]. Arsenite (As(III)) is the most toxic form of inorganic arsenic. It is present as uncharged arsenious acid in the pH range of 6.5–8.5, which makes it less amenable to adsorption compared to arsenate (As(V)) at the same pH range [2,3]. Therefore, oxidizing As(III) to As(V) was introduced as a viable way of improving inorganic As removal from water. Recent studies have provided an extensive explanation for the mechanism of oxidizing organic and inorganic As(III) to As(V). The oxidation process may be chemically achieved using ozone or iron and manganese compounds, microbiologically using *Herminiimonas arsenicoxydans* (known as ULPAs1) [4], or photochemically by applying ultraviolet radiation (UV) with or without activating agents such as TiO$_2$, H$_2$O$_2$ or sulfur [5].

With the predicted growth in the world's population, there is a global concern regarding the expected accompanying rise in waste disposal. For instance, increasing demands on the meat industry lead to an increase in the bone waste, particularly in countries that invest in livestock, such as Australia [6,7]. Exploring ways of utilizing these waste materials for different environmental applications can have a significant impact on protecting the environment in an economic and sustainable fashion. Incinerating the bone waste simultaneously produces energy and useful products such as bone char (BC). Bone char has been reported to have great potential for removing different contaminants from water [8,9]. Despite the high performance of bone char to remove fluoride and dyes from water, limited studies have examined its ability to remove As species, especially As(III). Thus, applying chemical and/or physical modification is crucial to improve its performance in this application [10].

Modification with nanomaterials is considered to be a promising method for improving the sorption capacity of adsorbents for water treatment because of their special physical and chemical properties. Some of these characteristics are related to their particle size and surface area, and photoelectronic and photocatalytic properties [11]. Metal-containing nanoparticles, carbonaceous nanomaterials, zeolites and dendrimers have been found to enhance sorption capacities of various adsorbents [12].

Titanium dioxide (or titania) nanoparticles are versatile, durable, and thermodynamically stable photocatalysts [13,14]. It has been reported to be a promising oxidative and reductive catalyst that is widely explored for removing organic and inorganic contaminants [12]. TiO_2 is mainly used as a semiconductor that can create a mobile electron by adsorbing the right amount of energy. Hence, it is commonly applied in combination with UV radiation. TiO_2 absorbs UV radiation with wavelengths of ~380 nm with a band-gap larger than 3.2 eV where the electron can move from the valence band to the conduction band [13–15]. TiO_2 is available in three different forms: anatase, rutile and brookite. Thermodynamically, rutile is the most stable form of TiO_2 with a higher surface energy than anatase which has the same particle size [16].

The photocatalyst activity of TiO_2 nanoparticles in oxidizing As(III) species was explored from different perspectives. For instance, Xu, et al. [15] reported that the methylated arsenic species were effectively oxidized by hydroxyl radicals formed in catalytic photolysis. Wei et al. [17] reported that high pH levels (11 and 12) are the optimum pH of the highest photocatalytic activity for three different facets of anatase. Guan et al. [18] reviewed the removal of As species using TiO_2. Their study revealed that TiO_2 had a low sorption capacity for As species at low concentrations. It is recommended that increasing the specific surface area and decreasing the degree of crystallinity may be applicable by supporting TiO_2 onto porous materials. This can also reduce the need for separating nanoparticles after treatment. Several studies introduced new composites such as TiO_2 with Ag_2O [19] or Fe_3O_4 [20] for As oxidation and removal from water. The present study is designed to evaluate the effect of UV radiation on concurrent arsenic oxidation and adsorption on a composite of $nTiO_2$ and bone char. To the knowledge of the authors, arsenic removal with simultaneous photocatalytic oxidation and adsorption with the composite has not been studied in previous research work, and this study attempts to provide some insight into this treatment process.

Based on the results achieved by our previous study that examined the effect of pyrolysis temperature in the range of 500–900 °C on As removal from water, BC pyrolyzed at 900 °C (BC900) was found to have the highest adsorption capacity for As species [10]. However, As(V) adsorption onto BC900 was more effective as opposed to As(III) under the same experimental conditions. Therefore, this bone char was selected to prepare the adsorptive catalytic composite to remove inorganic As from water without the need for pre-oxidation. The effectiveness of the composite for catalyzing the photo oxidation of As(III) was evaluated along with the overall adsorption capacity. The change in the absorbent structure with different treatment regimens was also tracked using a range of advanced analytical measurements.

2. Materials and Methods

2.1. Reagents and Equipment

Sheep bone samples (*Ovis aries*) were collected from local shop in Toowoomba, QLD, Australia. All reagents used were of analytical grade. Arsenite standard with a concentration of 1000 mg/L was purchased from Choice Analytical, New South Wales, Australia. Nitric acid (70%, RCI Labscan, NSW, Australia) and sodium hydroxide (Labscan Asia Co. Ltd., NSW, Australia) were used to control the pH of the solutions. TiO_2 nanoparticles (anatase, 99.9%, 18 nm) were purchased from US Research Nanomaterials, Inc. Potassium bromide was purchased from BDH Chemicals Ltd., Poole, England.

Arsenic assays were performed using Inductively Coupled Plasma Mass Spectrometry (ICP-MS) from PerkinElmer NEXION 300 (PerkinElmer, Shelton, CT, USA). ICP-MS hyphenated to Ultra-High Performance Liquid Chromatography (UHPLC) was used for arsenic speciation applying the method reported in [21]. Throughout the study, pH measurements were made using TPS smart Chem-Lab pH meter. The point of zero charge of the char samples was measured applying dynamic light scattering topology using a Nano-S Zetasizer (Malvern Instruments Ltd., Malvern, UK). After mixing 20 mg of bone char and 20 mL of water, the pH of the solution was adjusted in the range 3–10 using NaOH and HCl solutions following the same procedures reported in Alkurdi et. al. [10]. Ultrasonic cleaner model FXP 14 provided by Unisonic Australia Cleaning Systems, NSW, Australia was used for the composite preparation.

Pyrolysis process of bone char and the composite were performed using Rio Grande kiln, model CS2, USA. Surface morphology and the porous structure visualization of the samples were conducted using Scanning Electron Microscopy (SEM) (JEOL Ltd., model JCM-6000 Plus, Tokyo, Japan). The elemental surface analyses were carried out using SEM-EDS (JEOL JSM-7500FA) with accelerating voltage of 10 kV and probe current of 7.475 nA to detect the presence of Ti on the specimen. Reporting on the exact amount of Ti can be a bit of a challenge from an analytical point of view, as common measurement methods used in the literature such as X-ray fluorescence, FTIR and XRD are similar to EDS as they all provide qualitative results for Ti in solid state. Hence, the use of EDS is regarded as acceptable, and it is commonly applied in similar studies on coating and impregnation of adsorbents [22–24]. The composition and the functional groups were analyzed based on the results obtained from Fourier Transform Infrared (FTIR) spectroscopy (IRAffinity-1S FTIR spectrometer, Shimadzu, Kyoto, Japan) following the same procedure for the characterization of the BC900 reported in our previous work [10]. UV light was applied using 4-W Mini Ultra-violet Fluoro Lights (λ_{max} = 360 nm). The surface area, pore size and volume were performed by Particle and Surface Science Pty Limited. BET surface area was estimated from the results of N_2 adsorption at 77.3 K using Brunauer-Emmer-Teller.

2.2. Adsorbent Preparation

Bone char samples used in this study were the same as those tested in our previous study [10]. Two different procedures were followed for the preparation of the composite. These are ultrasound-assisted method (composite denoted as $(BC/nTiO_2)_{US}$, where the US used to indicate the use of ultrasound technology) after the pyrolysis of the bone samples and during the pyrolysis of raw bone mixture with $nTiO_2$ (composite denoted as $(BC/nTiO_2)_P$, where the P refers to "pyrolysis").

For the preparation of $(BC/nTiO_2)_{US}$, $nTiO_2$ slurry was prepared by adding 1 g of $nTiO_2$ nanoparticles to 100 mL double distilled water. The slurry was then stirred for 4 h to disperse and suspend the particles in the solution [25]. Thereafter, $nTiO_2$ slurry was shaken for 30 min in ultrasonic cleaner along with 5 g of BC900 (1–2 mm size) that was previously washed repeatedly using distilled water. The washing process was continued until the electrical conductivity was low and stable, indicating the removal of the mineralized ash. The composite was separated using filtration and then dried at 120 °C for 2 h. Afterward, the resultant solids were calcinated at 300 °C for 2 h [25] to obtain the final $(BC/nTiO_2)_{US}$

composite. This temperature was selected to avoid any further changes in the structure of the calcinated bone char and the transformation of anatase to rutile.

The second composite ($(BC/nTiO_2)_P$) was prepared following a simplified one step method. Briefly, 1 g $nTiO_2$ was added to 5 g of cleaned crushed bone pieces. Bone samples were crushed manually into about 1 cm^2 and boiled in tap water repeatedly in pressure cooker until all the fats and marrows were completely removed. Then, the mixture was sprayed with 20 mL distilled water to instigate the adhesion of $nTiO_2$ particles onto the cleaned bone. Next, the resultant product was placed in the kiln at 900 °C for 1 h. Later, the sample was grinded into 1–2 mm in diameter, washed with distilled water thoroughly to remove the excess nanoparticles on the surface and then dried at 60 °C for 24 h. The prepared two composite materials were sealed in plastic bags for later use in the adsorption experiments to avoid moisture entrapment into the composite.

2.3. Adsorbent Experiments

2.3.1. Experimental Setup

The setup used in this study for carrying out the experiments is illustrated in Figure 1. UV light was applied through three lamps with power of 4 W for each lamp [26]. The solution and the adsorbent were placed in a glass beaker (300 mL) and stirred using a magnetic stirrer. In order to avoid the breakage of the composite particles due to the friction between the magnetic bar and the bottom of the beaker, a vent cowl with metal mesh was used to cover the bar while conveying the stirring motion to the solution. Three power levels were tested in this study: 4, 8 and 12 W. For the 4 W test, the lamp was fixed on top of the beaker, whereas for the 8 and 12 W tests, the lamps were secured around the beaker at fixed distance between them.

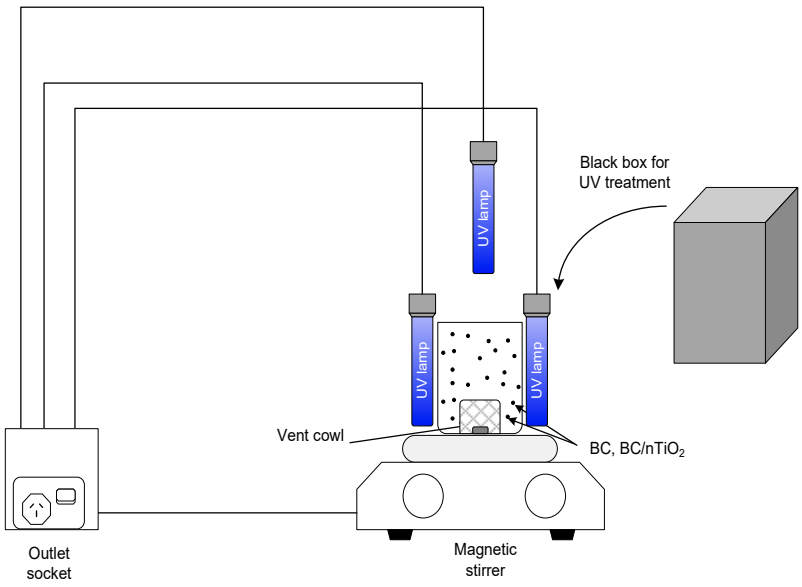

Figure 1. Experimental setup.

2.3.2. Experimental Procedure

Adsorption experiments were performed to examine the ability of the composite to remove As species from water compared to that of the uncoated BC900. The oxidation of arsenite under the effect of photolysis and photo-catalytic treatments was also examined. Adsorption experiments were performed by adding 5 g/L of the adsorbent to 100 mL of As(III) solution (2.5 mg/L) and mixed for 4 h at pH 8. The experimental conditions were selected based on a thorough kinetic experimental work on arsenic adsorption with BC900. A summary of the kinetic study outcome is provided in Table 1. For UV treatment, a black box was used to cover the solution to prevent the interference of natural light effects.

In order to compare the effect of coating with $nTiO_2$ on BC900, the same experimental conditions were applied with both BC900 and the coated BC900. After the elapse of reaction time, stirring was halted and samples were filtrated and analyzed for the residual As in solution to calculate the removal capacity applying the following formula:

$$q = \frac{C_0 - C_f}{D} * V \quad (1)$$

where q is the removal capacity in mg/g, C_0 is the initial concentration in mg/L, C_f is the final concentration, V is the solution volume (L) and D is the adsorbent dose in g/L.

Table 1. Optimum operating conditions for As species removal with BC900.

Experimental Condition	Range	As Species	
		As(III) Optimum	As(V) Optimum
Initial concentration (mg/L)	0.5–50	Maximum removal of 45.99% at 2.5 mg/L	Maximum removal of 55.29% at 1 mg/L
pH	4–10	8.6	7.5
Contact time (h)	0–12	4	4
Bone char dose (g/L)	2.5, 5 and 7.5	5	5

To examine the effect of UV light power on the oxidation of arsenite in the presence of TiO_2, a speciation procedure was carried out using HPLC/ICP-MS as mentioned earlier [20]. As(III) oxidation under the effect of UV light alone was not conducted as oxidation with the small UV power applied is insignificant especially in an unoptimized system configuration where UV losses could be high [27]. If oxidation occurred at all, the produced As(V) would very small and hard to detect. All the results are presented in mean values of three repeats for each experiment, except for the UHPLC analysis, where only two repeats were analyzed.

3. Results and Discussion

3.1. BC/nTiO$_2$ Characteristics

The efficiency of the two composite preparation methods for improving As adsorption was investigated through preliminary tests. It was found that $(BC/nTiO_2)_P$ was more effective than $(BC/nTiO_2)_{US}$. Hence, only $(BC/nTiO_2)_P$ is characterized here using a range of analytical measurements. However, FTIR analysis is an exception where comparison between the spectra of $(BC/nTiO_2)_{US}$ and $(BC/nTiO_2)_P$ are presented due to the observed interesting shifts in the peaks for the two composites.

The adherence of $nTiO_2$ onto bone char surface was confirmed using EDS analysis for BC900 and $(BC/nTiO_2)_P$ as shown in Figure 2. It can clearly be seen that there is a fair amount of Ti detected on the $(BC/nTiO_2)_P$ composite, indicating that this method was effective for preparing such a composite.

$(BC/nTiO_2)_P$ was also characterized for the surface pH, surface area, pore volume and pore size as presented in Table 2. Compared to the bone char pyrolyzed under the same conditions, the BET surface area was about half of that of the BC900's (69 m^2/g). Similarly, the pore volume was reduced from 0.24 cm^3/g to 0.16 cm^3/g for $(BC/nTiO_2)_P$ compared to BC900. However, the pore size was higher for $(BC/nTiO_2)_P$, 17 nm as opposed to 14 nm for BC900 [10]. The SEM images presented in Figure 3 show that the morphology of the char surface became rougher after the deposition of $nTiO_2$ particles. The pores on $(BC/nTiO_2)_P$ surface were larger but less dense in number compared to BC900 and this agrees with the results presented in Table 2. Similar results were observed by a recent study on coating activated carbon with copper where surface area and pore volume decreased while pore diameter increased with coating [28].

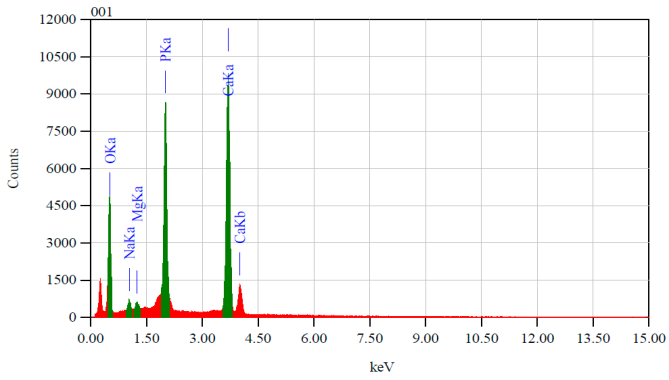

Elements	Mass %
C	4.07
O	41.15
Ca	34.00
P	19.7
Mg	0.66
Na	0.42

(a)

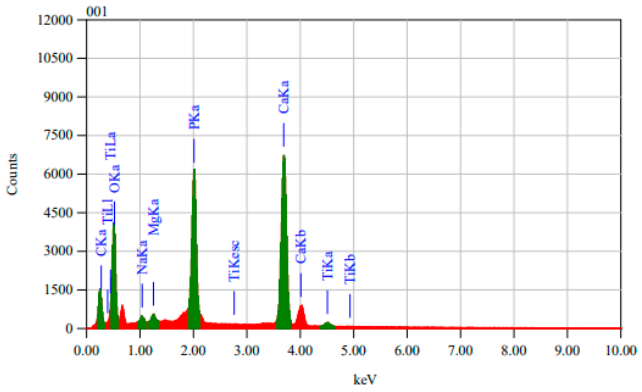

Elements	Mass %
C	4.08
O	39.62
Ca	35.38
P	18.76
Mg	0.58
Na	0.49
Ti	1.08

(b)

Figure 2. EDS analyses for (**a**) BC900 and (**b**) $(BC/nTiO_2)_P$.

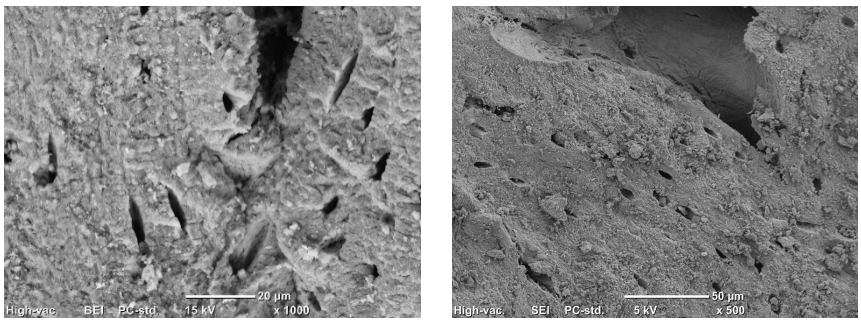

(a)

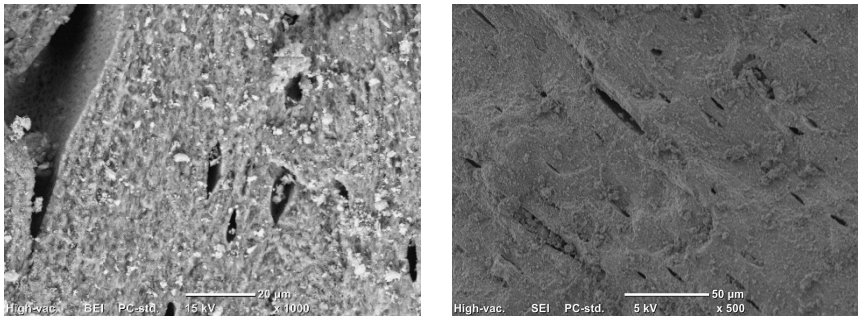

(b)

Figure 3. SEM images for (**a**) BC900 and (**b**) $(BC/nTiO_2)_P$.

Table 2. $(BC/nTiO_2)_P$ characteristics.

Pyrolysis Temperature (°C)	900
Surface pH	9.9
pH_{pzc}	3.82 and 8.79
BET Surface Area (m^2/g)	38
Pore Volume (cm^3/g)	0.16
Pore Size (nm)	17

The surface charge of $(BC/nTiO_2)_P$ was also examined and the results are depicted in Figure 4. The composite surface charge at its initial pH was −9.03 mV. This value increased after reducing the pH of the solution down to pH 5, and then dropped as pH decreased to provide two points of zero charge (pH_{pzc}) at 3.82 and 8.79. Similar results were achieved by Deng et al. [29] after deposition of conductive polymers on TiO_2 surface. These results are also comparable to the results reported by Kaya and Yukselen [30], as they showed that the zeta potential has two points of zero charge because they follow the diffuse electrical double-layer theory. Thus, in the case of the coated bone char, one is due to the bone char and the other is related to the $nTiO_2$. It has been reported in the literature that the presence of divalent cations results in two points of zero charge when they exist at high concentrations [31]. However, this is unlikely applicable in the case of the coated bone char as it was not detected in the case of the uncoated char (BC900). In comparison, BC900 has only one pH_{pzc} at a pH of ~8.3 [10]. This means that at the selected pH of 8 for the adsorption experiments, $(BC/nTiO_2)_P$ is positively charged, while BC900′ surface carries a slight negative charge. This gives $(BC/nTiO_2)_P$ the competitive edge over BC900 when it comes to electrostatic interaction between negatively charged As species and adsorbents.

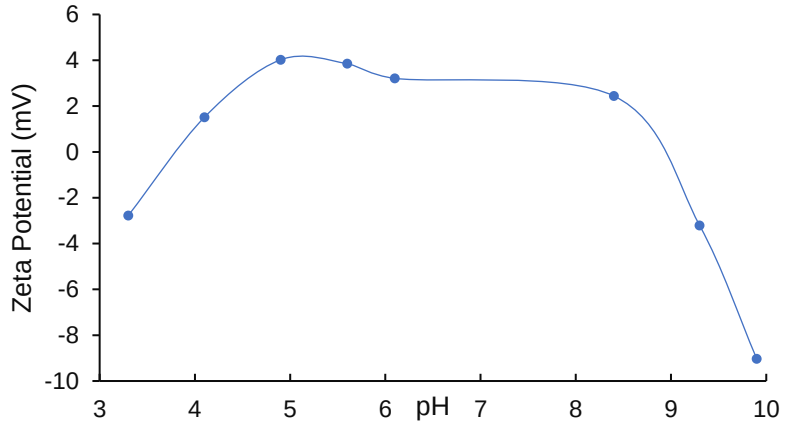

Figure 4. $(BC/nTiO_2)_P$ surface charge at various pH levels.

FTIR analysis was carried out to detect the changes which resulted after depositing of $nTiO_2$ particles onto the BC900. Figure 5 shows that the deposition of $nTiO_2$ particles decreased the signal of functional groups present on the surface. The composite $(BC/nTiO_2)_{US}$ exhibited a significant decrease in the peaks related to the presence of amide groups and the oxygen containing groups in the range 1585–1700 cm^{-1}. It was established that these groups are likely to be related to bone protein decomposition during pyrolysis [10]. This indicates that TiO_2 interacts with these groups during pyrolysis, and this led to the disappearance of their corresponding peaks. This is supported by the findings of Roguska et al. [32], who reported a high adsorption capacity of protein onto TiO_2. However, these peaks changed only a little for the case of $(BC/nTiO_2)_P$. This may be related to the decomposition of the protein in the first stage of the pyrolysis process and less interaction of TiO_2 at a lower temperature (300 °C).

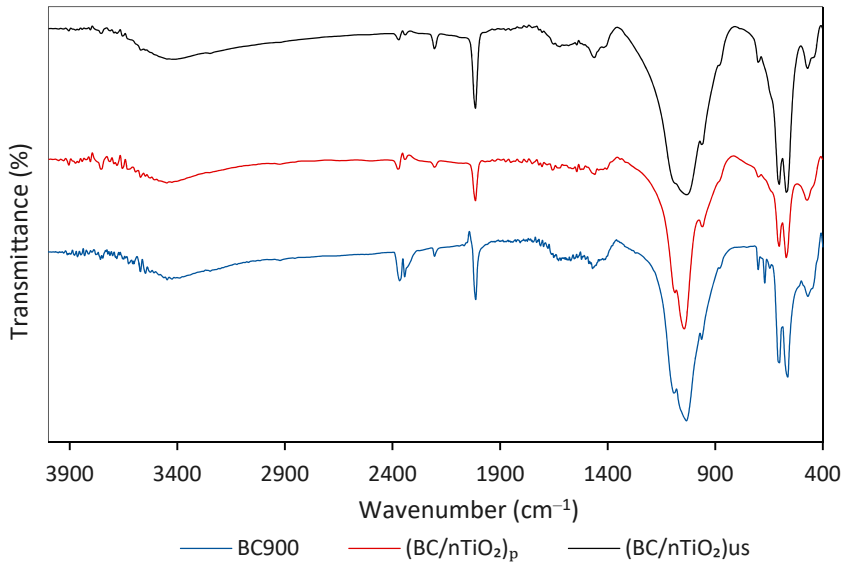

Figure 5. FTIR spectra of BC900 and its composites prepared following two different procedures.

Compared to BC900, the peaks associated with PO_4^{3-} shifted slightly from 1032 to 1041 cm^{-1}, 962 to 956 cm^{-1} and 563 to 570 cm^{-1} after TiO_2 deposition. Similarly, the peaks at 1408 and 880 cm^{-1} that are related to CO_3^{2-} shifted to 1420 and 887 cm^{-1}. In addition, the peak of the hydroxyl group shifted from 3443 to 3448 cm^{-1} due to the deposition of $nTiO_2$ particles. The shifting in the position of the main peaks of the composite compared to BC900 highlights the change in the BC structure due to $nTiO_2$ particles deposition onto the char surface. Furthermore, the reduction in the BET surface area and pore volume is further evidence of the incorporation of the nanoparticles into the bone char structure. FTIR spectrum of $(BC/nTiO_2)_{US}$ showed the formation of a small peak at 1342 cm^{-1}, due to the formation of a Ti-O-Ti bond [33,34]. Depositing $nTiO_2$ particles after pyrolysis resulted in a broader peak of PO_4^{3-} at 1033 cm^{-1} and a higher intensity for the peaks related to the presence of PO_4^{3-} at 570 and 601 cm^{-1}. This may be related to the formation of new complexes between PO_4^{3-} and the nanoparticles.

The difference in the properties of the composites prepared during or after pyrolysis conditions can be attributed to the effect of temperature on $nTiO_2$. For the case of $(BC/nTiO_2)_P$, TiO_2 was exposed to a temperature of 900 °C, which probably resulted in the transformation of the photocatalyst from anatase to rutile as such a transformation was reported to occur at 600 °C [35]. In comparison, the anatase in the composite $(BC/nTiO_2)_{US}$ was exposed only to 300 °C, and hence TiO_2 remained in its original polymorph. The transformation of $nTiO_2$ from anatase to rutile form was confirmed by taking the FTIR spectra for the $nTiO_2$ before and after exposure to 900 °C and compare it with the spectra of previous studies as demonstrated in Figure 6. The analogy between the spectra obtained for $nTiO_2$ before and after pyrolysis at 900 °C in this study and those reported by Kalaivani and Anilkumar [36] is clear. It seems that anatase form has a few characteristic peaks that contracted to one characteristic peak as it transformed to rutile.

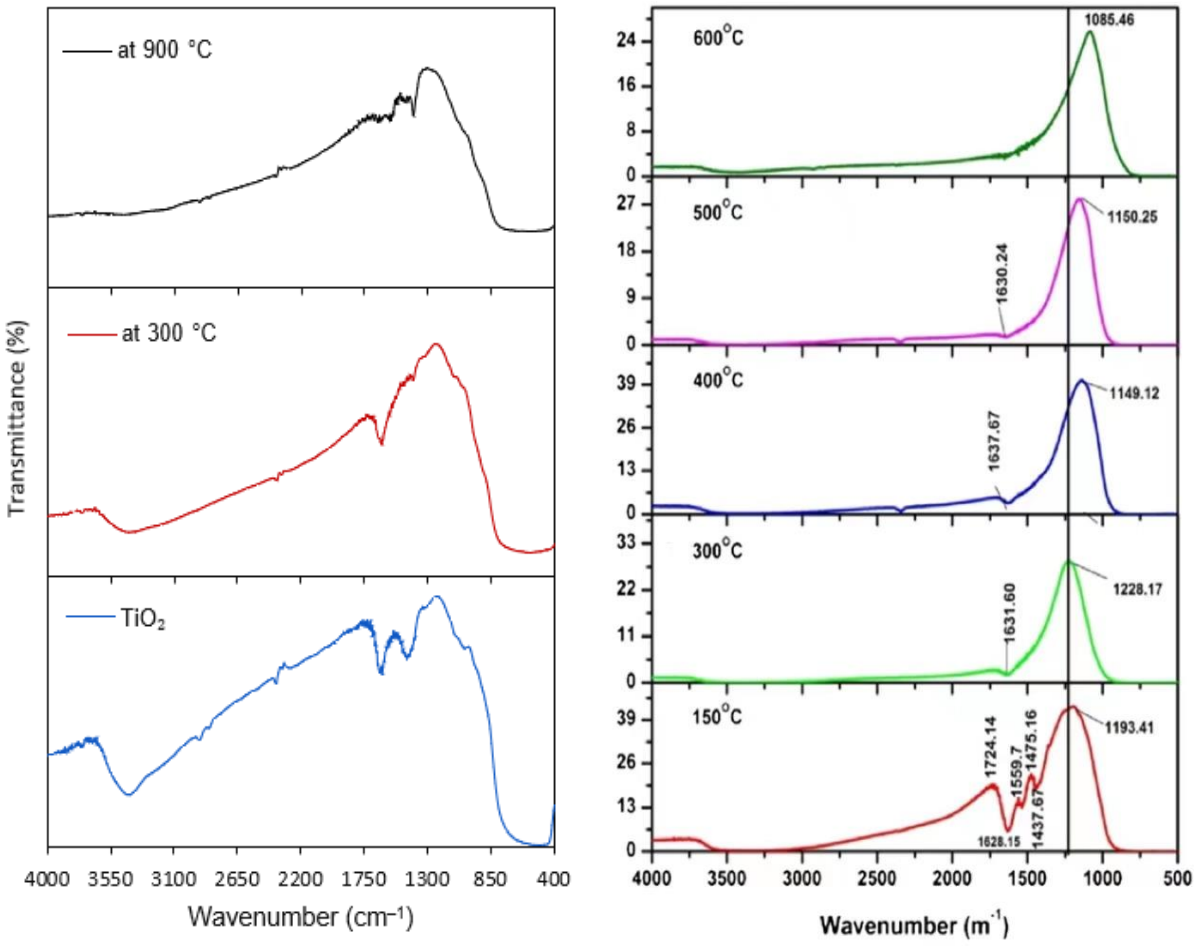

(a) (b)

Figure 6. FTIR spectra for (**a**) $nTiO_2$ before and after exposure to 300 °C and 900 °C in this study and (**b**) TiO_2 transformation with temperature from anatase to rutile. Adapted from Ref. [36].

3.2. Arsenic Adsorption

The initial As(III) concentration was measured to check for any oxidation that might have happened due to solution mixing. The first step of the adsorption experiments involved comparing the two composites' efficiency in removing As in the presence of 12 W UV light source. Figure 7 shows arsenic speciation for untreated and treated samples with the two composites. It can be seen that the arsenite adsorption capacity (indicated by the total concentration) and oxidation with $(BC/nTiO_2)_P$ was higher than that of $(BC/nTiO_2)_{US}$. The adsorption capacity of the former was 57.3% compared to 24.8% for the latter. Recent studies compared the removal of As(III) and As(V) on the two phases of $nTiO_2$ (namely anatase and rutile) and reported that anatase had a higher removal capacity compared to rutile [37,38]. However, in our study, the reverse action was observed, as the TiO_2 exposed to 900 °C (rutile form) was more efficient than that exposed to 300 °C (anatase form). This suggests that TiO_2 behaves differently when interacting with bone char. The composite of rutile with bone char creates a more effective adsorbent than the composite of anatase with bone char. Based on the measured residual arsenate after adsorption, the oxidation with $(BC/nTiO_2)_P$ was about 3.5 times higher than that of $(BC/nTiO_2)_{US}$.

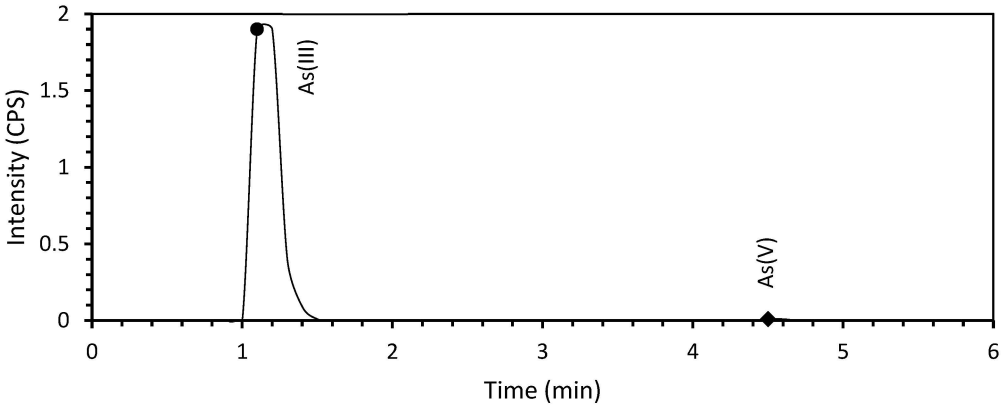

Retention Time (min)	Component Name	Isotope	Area	Height	Concentrations	Units
1.185	As(III)	As 75	15,106,266	2,286,023	2.457	ppm
3.442		As 75	6715	300		
4.059		As 75	2045	204		
4.555	As(V)	As 75	274,035	19,787	0.022	ppm
5.728		As 75	3029	257		
Total			15,392,091		2.479	

(**a**)

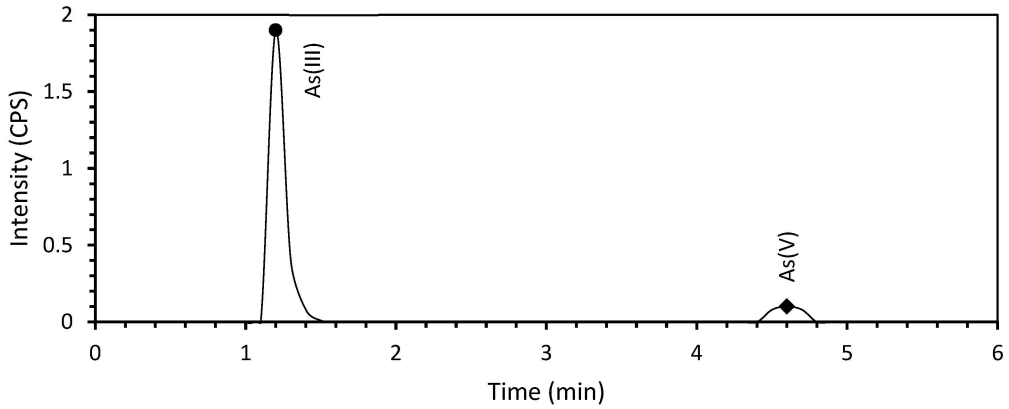

Retention Time (min)	Component Name	Isotope	Area	Height	Concentrations	Units
0.305		As 75	4155	216		
0.850		As 75	1363	241		
1.198	As(III)	As 75	11,645,912	2,227,567	1.74	ppm
2.931		As 75	11,979	357		
3.414		As 75	6585	256		
4.594	As(V)	As 75	1,408,336	103,798	0.12	ppm
Total			13,078,330		1.87	

(**b**)

Figure 7. *Cont.*

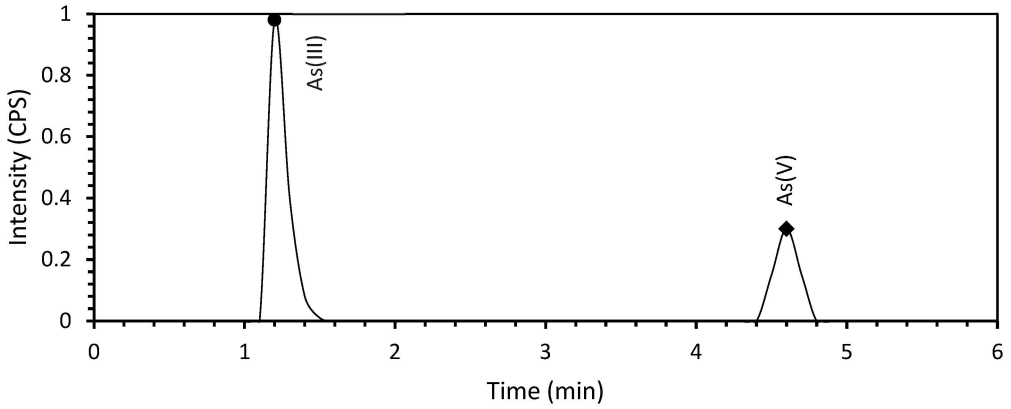

Retention Time (min)	Component Name	Isotope	Area	Height	Concentrations	Units
0.33		As 75	2867	350		
1.199	As(III)	As 75	6,320,417	1,056,795	0.65	ppm
3.286		As75	12,373	318		
4.583	As(V)	As75	3,706,422	276,743	0.41	ppm
Total			10,042,079		1.06	

(**c**)

Figure 7. Arsenic speciation for (**a**) untreated sample, (**b**) treated sample with UV and $(BC/nTiO_2)_{US}$, (**c**) treated sample with UV and $(BC/nTiO_2)_P$.

Considering the abovementioned results, $(BC/nTiO_2)_P$ was used to further investigate the effect of UV power level on arsenic adsorption capacity. These tests were compared with treatments of BC900 alone and $(BC/nTiO_2)_P$ with visible light to evaluate UV effect on arsenic adsorption. Figure 8 compares the removal capacity of As species using the same composite at different power levels with UV light (4, 8, and 12 W). In addition, As removal capacity of UV light treatments were compared to that of the uncoated bone char and those of the coated bone char in the absence of UV light to gauge the impact of UV light addition to the removal process. Increasing UV power from 4 to 8 increased the As adsorption capacity of the solution from 117 to 123 μg/g. Further increase of UV power to 12 W resulted in the highest adsorption capacity of 281 μg/g. Surprisingly, the adsorption capacity of the $(BC/nTiO_2)_P$ with visible light was slightly higher than those of 4 and 8 W of UV light. This indicates that the minimum UV light required to enhance the adsorption capacity was 12 W per 100 mL for water with arsenic concentration of 2.5 mg/L. BC900 adsorption capacity in Figure 8 represents the contribution of adsorption to the removal while other treatments represent the combined effects of oxidation and adsorption. It can be noticed that BC900 had better adsorption capacity than $(BC/nTiO_2)_P$ with low UV power and visible light. This could be ascribed to the loss of surface area and pore volume due to TiO_2 deposition. In order to make up for the loss of these traits, high UV power needs to be applied to obtain better removal outcome. It should be noted that even with the chemical modification of bone char and UV application, the maximum removal (281.4 μg As/g of $(BC/nTiO_2)_P$) could not bring down the concentration of arsenic to the acceptable limit for human consumption (i.e., 10 μg/L based on WHO recommendation). This can probably be achieved by increasing the adsorbent dosage and the contact time and with lower As initial concentration. Bone char alone (BC900) achieved arsenic adsorption capacity of 196 μg/g. Although the increase in the adsorption capacity with $nTiO_2$ modification and UV application is little considering the cost associated with these additions, thorough investigation for the removal mechanisms and kinetics of $(BC/nTiO_2)_P$ + UV is required to draw a firm conclusion regarding the feasibility of this process for arsenic removal. In

comparison to commercially available adsorbents such as GHE and Bayoxide and their high arsenic removal capacity [39,40], bone char might score low. However, bone char has the advantage of being sourced from waste and as a by-product of energy producing processes (i.e., gasification [6]) as well as its ability to be regenerated and reused. These traits make it worth investigation for future potential use for arsenic removal under different environmental conditions.

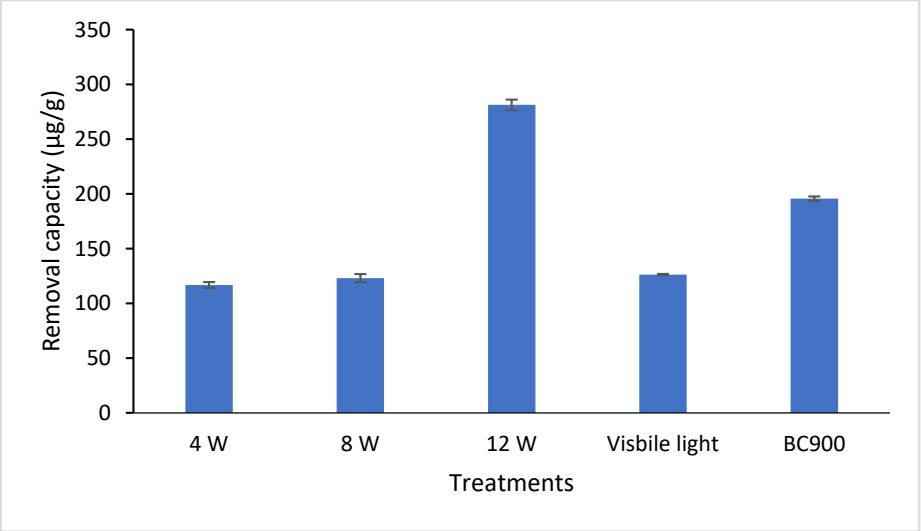

Figure 8. As removal capacity with different treatment scenarios. Experimental conditions: pH = 8, As(III) initial concentration = 2.5 mg/L, adsorbent dose = 5 g/L.

The changes in bone char and $(BC/nTiO_2)_P$ structure after As loading and exposure to UV radiation was studied using FTIR analysis and the results are presented in Figure 9. The most prominent peak in Figure 9a is the peak at 1381 cm^{-1}. This peak is assigned to the presence of nitro compounds [41]. The formation of this peak is accompanied by the reduction of the peak at 2013 cm^{-1}, which is assigned to the cyanate compounds that were formed due to the decomposition of the protein in the bone structure at high pyrolysis temperature [10]. The peak at 1647 cm^{-1} was found to be linked to sodium arsenate [42] and this suggests that an interaction between arsenate and the sodium in the bone char structure might have occurred. Sometimes peaks in the 1600 cm^{-1} region are ascribed to adsorbed water [43]. However, in the case of this study, a prominent peak only appeared for the loaded composite, confirming that it is related to As interaction with the composite structure. The increased intensity of the broad OH peak at 3425 cm^{-1} is due to the high potency of TiO_2 to attract OH. The reduction in the intensity of the peak related to the presence of PO_4^{3-} at 1033 cm^{-1} suggests the possibility of ion contribution to the removal process. The change in the peak's intensity and width in the region 400–1000 cm^{-1} is believed to be due to As interaction with oxygen-containing moieties on the char surface [44,45].

Figure 9b shows the differences in the adsorbents' composition after they were loaded with As species in different treatment scenarios. It appears that UV improves the decomposition of cyanate and promotes the formation of nitro compounds represented by the diminishing peak at 2013 cm^{-1} and the rise of the peak at 1380 cm^{-1}. The other obvious effect of UV is the change in the spectra for wavenumber less than 1000 cm^{-1}, and this could be due to the formation of hydroxyl radicals in the photocatalytic decomposition of water molecules and the reaction of the latter with arsenic forming As-O compounds on the char.

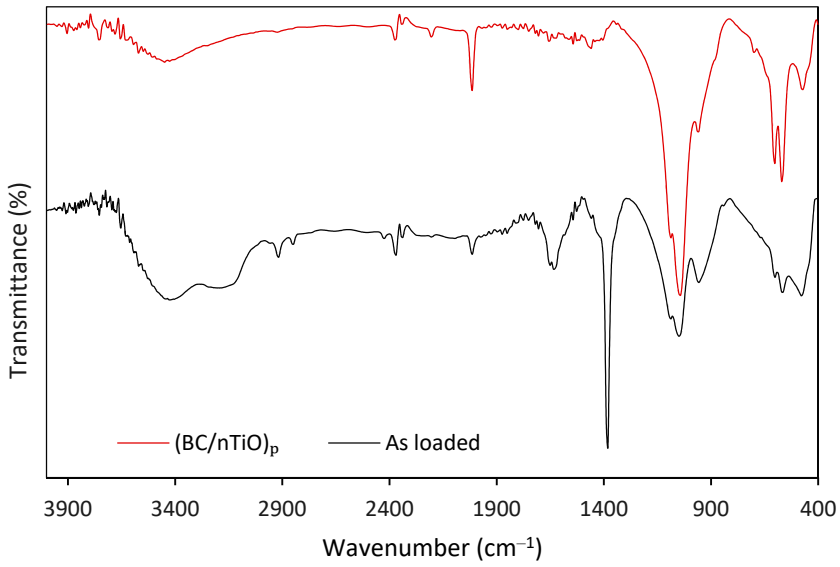

(**a**)

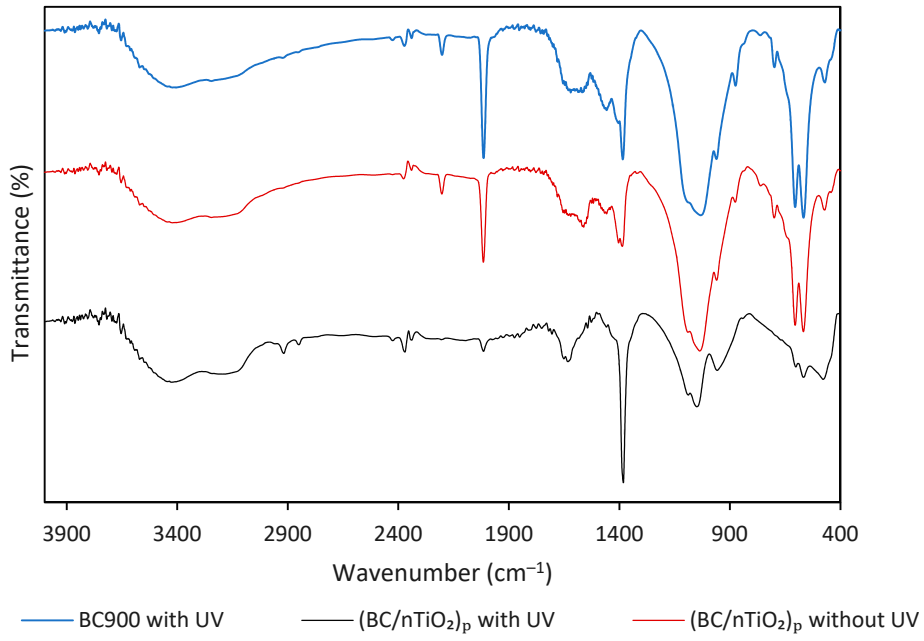

(**b**)

Figure 9. FTIR analysis for (**a**) As loading effect on $(BC/TiO_2)_P$ structure and (**b**) UV and $nTiO_2$ effect on BC900 structure.

As removal in $BC/nTiO_2$ may be explained based on the removal mechanism of bone char itself and those for the nano TiO_2 particles. Based on our earlier work on bone char, we found that the removal of As species is mainly governed by surface complexation as the predominate mechanism of the removal. Precipitation is also expected to participate in the removal [10]. On the other hand, arsenic removal on TiO_2 may follow two different mechanisms. TiO_2 may act as an adsorbent for As(III) and As(V) following surface to complexation mechanism due to the formation of $Ti_2AsO_4^-$ and $Ti_2AsO_3^-$, respectively [46]. The second mechanism is the photocatalytic activity of TiO_2, which was found effectively contribute to As(III) oxidation. This process is likely to be the main removal mechanism

in the presence of UV radiation [18]. By adsorbing UV light with a band-gap larger than 3.2 eV, the electrons can move from the valence band to the conduction band [15]. As a result, bone char engineered by $nTiO_2$ is likely to provide enhanced sorption photocatalytic capabilities associated with Ti-C, Ti-O and Ti-O-Ti groups on the surface.

4. Conclusions and Recommendations for Future Actions

A composite of bone char and TiO_2 nanoparticles was prepared following two different procedures: $nTiO_2$ addition during and after pyrolysis. The two composites were compared for their effectiveness in removing inorganic As from the aqueous solution with the aid of UV. The composite $(BC/nTiO_2)_P$ proved to be more effective in arsenite removal (57.3% vs. 24.8%) and photocatalytic oxidation (3.5 times higher arsenate produced). Arsenic removal using $(BC/nTiO_2)_P$ and UV power of 4, 8 and 12 W was tested and compared to the treatment with visible light and BC900. It was found that power levels of 4 and 8 W had a lower As adsorption capacity than that of $(BC/nTiO_2)_P$ with visible light and BC900. It was concluded that the loss of bone char surface area and pore volume due to $nTiO_2$ deposition can only be compensated by applying high UV power. FTIR analysis of the loaded $(BC/nTiO_2)_P$ composite with As suggested that removal occurred due to interaction with sodium, hydroxyl radicals and possibly PO_4. This study showed that depositing $nTiO_2$ onto bone char and applying UV radiation was successful in achieving simultaneous dual effects of oxidation and adsorption. Further studies for identifying arsenic removal mechanisms and kinetics and isotherms with $(BC/nTiO_2)_P$ and UV are recommended for future research work. Testing different parameters to achieve low As concentrations that meet regulatory limits is a valuable goal for developing this work further.

Author Contributions: S.A. contributed to the conceptualization of the research idea, conducted experiments, data collection, analyses and put together the original draft. R.A.-J. provided support and guidance during the experimental work, performed EDS analyses, contributed to data analysis and revised and amended the final draft. J.B. contributed to the conceptualization of the research idea and provided supervision and guidance during the experimental work. A.M. provided support for arsenic speciation and measurements. All authors have read and agreed to the published version of the manuscript.

Funding: This research was funded by the Iraqi Government and the Australian Research Training Program.

Institutional Review Board Statement: Not applicable, the sheep bones used in this research were obtained from a commercial, approved, butcher who is selling sheep meet to the population in Australia (fulfilling all legislative approvals).

Informed Consent Statement: Not applicable.

Data Availability Statement: Data sharing not applicable.

Acknowledgments: This research was performed as a part of PhD research which was supported in part by the Iraqi Government and the Australian Research Training Program. The authors are thankful to Prasanna Kumarathilaka for his contribution and support in As speciation using UHPLC.

Conflicts of Interest: The authors declare no conflict of interest. The funders had no role in the design of the study; in the collection, analyses, or interpretation of data; in the writing of the manuscript, or in the decision to publish the results.

References

1. Kumarathilaka, P.; Seneweera, S.; Ok, Y.-S.; Meharg, A.A.; Bundschuh, J. Mitigation of arsenic accumulation in rice: An agronomical, physico-chemical, and biological approach—A critical review. *Crit. Rev. Environ. Sci. Technol.* **2020**, *50*, 31–71. [CrossRef]
2. Clifford, D.; Ghurye, G. Oxidizing Arsenic III to Arsenic V for Better Removal. Water Quality Product. 2001, pp. 28–29. Available online: https://www.wwdmag.com/groundwater/oxidizing-arsenic-iii-arsenic-v-better-removal (accessed on 27 October 2021).
3. Zeltner, W.A. *Simultaneous Removal of Arsenite As (III) and Arsenate As (V) From Drinking Water Using a Novel Photoactive Adsorbent*; EPA: Washington, DC, USA, 2002.

4. Weiss, S.; Carapito, C.; Cleiss, J.; Koechler, S.; Turlin, E.; Coppee, J.-Y.; Heymann, M.; Kugler, V.; Stauffert, M.; Cruveiller, S.; et al. Enhanced structural and functional genome elucidation of the arsenite-oxidizing strain Herminiimonas arsenicoxydans by proteomics data. *Biochim.* **2009**, *91*, 192–203. [CrossRef]
5. Bissen, M.; Frimmel, F.H. Arsenic—A Review. Part II: Oxidation of arsenic and its removal in water treatment. *Acta Hydrochim. Hydrobiol.* **2003**, *31*, 97–107. [CrossRef]
6. Alkurdi, S.S.A.; Al-Juboori, R.A.; Bundschuh, J.; Hamawand, I. Bone char as a green sorbent for removing health threatening fluoride from drinking water. *Environ. Int.* **2019**, *127*, 704–719. [CrossRef] [PubMed]
7. OECD/FAO. *OECD-FAO Agricultural Outlook 2018–2027*; OECD: Paris, France; FAO: Rome, Italy, 2018.
8. Minja, R. Practical approach for removal of natural organic matter and defluoridation of Maji ya Chai river water: Use of acid pre-treated bone char and coagulants. *Tanzan. J. Eng. Technol.* **2019**, *38*, 204–206. [CrossRef]
9. Rojas-Mayorga, C.K.; Albero, J.S.; Aguayo, I.; Castillo, D.I.M.; Bonilla-Petriciolet, A. A new synthesis route for bone chars using CO_2 atmosphere and their application as fluoride adsorbents. *Microporous Mesoporous Mater.* **2015**, *209*, 38–44. [CrossRef]
10. Alkurdi, S.S.; Al-Juboori, R.A.; Bundschuh, J.; Bowtell, L.; McKnight, S. Effect of pyrolysis conditions on bone char characterization and its ability for arsenic and fluoride removal. *Environ. Pollut.* **2020**, *262*, 114221. [CrossRef] [PubMed]
11. Liu, Y.; Su, G.; Zhang, B.; Jiang, G.; Yan, B. Nanoparticle-based strategies for detection and remediation of environmental pollutants. *Anal.* **2011**, *136*, 872–877. [CrossRef]
12. Savage, N.; Diallo, M.S. Nanomaterials and water purification: Opportunities and challenges. *J. Nanoparticle Res.* **2005**, *7*, 331–342. [CrossRef]
13. Hashimoto, K.; Irie, H.; Fujishima, A. TiO_2 Photocatalysis: A historical overview and future prospects. *Jpn. J. Appl. Phys.* **2005**, *44*, 8269. [CrossRef]
14. Woan, K.; Pyrgiotakis, G.; Sigmund, W. Photocatalytic carbon-nanotube-TiO_2 composites. *Adv. Mater.* **2009**, *21*, 2233–2239. [CrossRef]
15. Xu, T.; Cai, A.Y.; O'Shea, K.E. Adsorption and photocatalyzed oxidation of methylated arsenic species in TiO_2 suspensions. *Environ. Sci. Technol.* **2007**, *41*, 5471–5477. [CrossRef] [PubMed]
16. Mancardi, G.; Tamargo, C.H.; Terranova, U.; de Leeuw, N.H. Calcium phosphate deposition on planar and stepped (101) surfaces of anatase TiO_2: Introducing an interatomic potential for the TiO_2/Ca-PO_4/water interface. *Langmuir* **2018**, *34*, 10144–10152. [CrossRef]
17. Wei, Z.; Fang, Y.; Wang, Z.; Liu, Y.; Wu, Y.; Liang, K.; Yan, J.; Pan, Z.; Hu, G. pH effects of the arsenite photocatalytic oxidation reaction on different anatase TiO_2 facets. *Chemosphere* **2019**, *225*, 434–442. [CrossRef] [PubMed]
18. Guan, X.; Du, J.; Meng, X.; Sun, Y.; Sun, B.; Hu, Q. Application of titanium dioxide in arsenic removal from water: A review. *J. Hazard. Mater.* **2012**, *215–216*, 1–16. [CrossRef]
19. Ren, H.-T.; Han, J.; Li, T.-T.; Sun, F.; Lin, J.-H.; Lou, C.-W. Visible light-induced oxidation of aqueous arsenite using facile Ag_2O/TiO_2 composites: Performance and mechanism. *J. Photochem. Photobiol. A Chem.* **2019**, *377*, 260–267. [CrossRef]
20. Deng, M.; Wu, X.; Zhu, A.; Zhang, Q.; Liu, Q. Well-dispersed TiO_2 nanoparticles anchored on Fe_3O_4 magnetic nanosheets for efficient arsenic removal. *J. Environ. Manag.* **2019**, *237*, 63–74. [CrossRef] [PubMed]
21. Herath, I.; Kumarathilaka, P.; Bundschuh, J.; Marchuk, A.; Rinklebe, J. A fast analytical protocol for simultaneous speciation of arsenic by Ultra-High Performance Liquid Chromatography (UHPLC) hyphenated to Inductively Coupled Plasma Mass Spectrometry (ICP-MS) as a modern advancement in liquid chromatography approaches. *Talanta* **2020**, *208*, 120457. [CrossRef]
22. Li, J.; Tian, B.; Li, T.; Dai, S.; Weng, Y.; Lu, J.; Xu, X.; Jin, Y.; Pang, R.; Hua, Y. Biosynthesis of Au, Ag and Au-Ag bimetallic nanoparticles using protein extracts of *Deinococcus radiodurans* and evaluation of their cytotoxicity. *Int. J. Nanomed.* **2018**, *13*, 1411–1424. [CrossRef]
23. Chen, L.; Liao, Y.; Chen, Y.; Wu, J.; Ma, X. Performance of Ce-modified VW-Ti type catalyst on simultaneous control of NO and typical VOCS. *Fuel Process. Technol.* **2020**, *207*, 106483. [CrossRef]
24. Motlochová, M.; Slovák, V.; Pližingrová, E.; Szatmáry, L.; Bezdička, P.; Šubrt, J. The influence of annealing temperature on properties of TiO_2 based materials as adsorbents of radionuclides. *Thermochim. Acta* **2019**, *673*, 34–39. [CrossRef]
25. Jia, B.-Y.; Duan, L.-Y.; Ma, C.-L.; Wang, C.-M. Characterization of TiO_2 loaded on activated carbon fibers and its photocatalytic reactivity. *Chin. J. Chem.* **2007**, *25*, 553–557. [CrossRef]
26. Yoon, S.-H.; Lee, J.H. Oxidation mechanism of As(III) in the UV/TiO_2 system: Evidence for a direct hole oxidation mechanism. *Environ. Sci. Technol.* **2005**, *39*, 9695–9701. [CrossRef] [PubMed]
27. Ghurye, G.; Clifford, D. Laboratory study on the oxidation of As (III) to As (V). National Risk Management Research Laboratory, Office of Research and Development, US Environmental Protection Agency. In Proceedings of the AWWA Water Quality Technology Conference, Houston, TX, USA, 1 March 2001; Volume 1, pp. 12–20.
28. Zhao, X.; Zhang, A.; Zhang, J.; Wang, Q.; Huang, X.; Wu, Y.; Tang, C. Enhanced selenate removal in aqueous phase by copper-coated activated carbon. *Mater.* **2020**, *13*, 468. [CrossRef] [PubMed]
29. Deng, F.; Min, L.; Luo, X.; Wu, S.; Luo, S. Visible-light photocatalytic degradation performances and thermal stability due to the synergetic effect of TiO_2 with conductive copolymers of polyaniline and polypyrrole. *Nanoscale* **2013**, *5*, 8703–8710. [CrossRef] [PubMed]
30. Kaya, A.; Yukselen, Y. Zeta potential of clay minerals and quartz contaminated by heavy metals. *Can. Geotech. J.* **2005**, *42*, 1280–1289. [CrossRef]

31. Hsu, J.-P.; Nacu, A. Behavior of soybean oil-in-water emulsion stabilized by nonionic surfactant. *J. Colloid Interface Sci.* **2003**, *259*, 374–381. [CrossRef]
32. Roguska, A.; Pisarek, M.; Andrzejczuk, M.; Dolata, M.; Lewandowska, M.; Janik-Czachor, M. Characterization of a calcium phosphate-TiO_2 nanotube composite layer for biomedical applications. *Mater. Sci. Eng. C* **2011**, *31*, 906–914. [CrossRef]
33. Kannaiyan, D.; Kochuveedu, S.T.; Jang, Y.H.; Jang, Y.J.; Lee, J.Y.; Lee, J.; Lee, J.; Kim, J.; Kim, D.H. Enhanced photophysical properties of nanopatterned titania nanodots/nanowires upon hybridization with silica via bock copolymer templated sol-gel process. *Polym.* **2010**, *2*, 490–504. [CrossRef]
34. Thamir, A.D.; Haider, A.J.; Ali, G.A. Preparation of nanostructureTiO_2 at different temperatures by pulsed laser deposition as solar cell. *Eng. Technol. J.* **2016**, *34*, 193–204.
35. Hanaor, D.A.H.; Sorrell, C.C. Review of the anatase to rutile phase transformation. *J. Mater. Sci.* **2011**, *46*, 855–874. [CrossRef]
36. Kalaivani, T.; Anilkumar, P. Role of temperature on the phase modification of TiO_2 nanoparticles synthesized by the precipitation method. *Silicon* **2018**, *10*, 1679–1686. [CrossRef]
37. Gupta, K.K.; Singh, N.L.; Pandey, A.; Shukla, S.K.; Upadayay, S.N.; Mishra, V.; Srivastava, P.; Lalla, N.P.; Mishra, P.K. Effect of anatase/rutile TiO_2 phase composition on arsenic adsorption. *J. Dispers. Sci. Technol.* **2013**, *34*, 1043–1052. [CrossRef]
38. Ma, L.; Tu, S.X. Removal of arsenic from aqueous solution by two types of nano TiO_2 crystals. *Environ. Chem. Lett.* **2011**, *9*, 465–472. [CrossRef]
39. Driehaus, W. Arsenic removal—experience with the GEH® process in Germany. *Water Supply* **2002**, *2*, 275–280. [CrossRef]
40. Katsoyiannis, I.A.; Mitrakas, M.; Zouboulis, A. Arsenic occurrence in Europe: Emphasis in Greece and description of the applied full-scale treatment plants. *Desal. Water Treat.* **2014**, *54*, 2100–2107. [CrossRef]
41. Janakiraman, N.; Johnson, M. Functional groups of tree ferns (Cyathea) using FTIR: Chemotaxonomic implications. *Rom. J. Biophys.* **2015**, *25*, 131–141.
42. Li, Z.; Hong, H.; Jean, J.-S.; Koski, A.J.; Liu, C.-C.; Reza, S.; Randolph, J.J.; Kurdas, S.R.; Friend, J.H.; Antinucci, S.J. Characterization on arsenic sorption and mobility of the sediments of Chia-Nan Plain, where Blackfoot disease occurred. *Environ. Earth Sci.* **2011**, *64*, 823–831. [CrossRef]
43. Rytwo, G.; Zakai, R.; Wicklein, B. The use of ATR-FTIR spectroscopy for quantification of adsorbed compounds. *J. Spectrosc.* **2015**, *2015*, 727595. [CrossRef]
44. Cowen, S.; Duggal, M.; Hoang, T.; Al-Abadleh, H.A. Vibrational spectroscopic characterization of some environmentally important organoarsenicals—A guide for understanding the nature of their surface complexes. *Can. J. Chem.* **2008**, *86*, 942–950. [CrossRef]
45. Min, X.; Li, Y.; Ke, Y.; Shi, M.; Chai, L.; Xue, K. Fe-FeS_2 adsorbent prepared with iron powder and pyrite by facile ball milling and its application for arsenic removal. *Water Sci. Technol.* **2017**, *76*, 192–200. [CrossRef] [PubMed]
46. Pena, M.; Meng, X.; Korfiatis, G.P.; Jing, C. Adsorption mechanism of arsenic on nanocrystalline titanium dioxide. *Environ. Sci. Technol.* **2006**, *40*, 1257–1262. [CrossRef] [PubMed]